Available online at www.sciencedirect.com
ScienceDirect
ELSEVIER
International Journal of Fatigue xxx (2007) xxx–xxx
International Journal of Fatigue
www.elsevier.com/locate/ijfatigue

The influence of grains' crystallographic orientations on advancing short crack

Igor Simonovski *, Leon Cizelj

Jožef Stefan Institute, Reactor Engineering Division, Jamova 39, SI-1000 Ljubljana, Slovenia

Received 31 August 2006; received in revised form 16 January 2007; accepted 31 January 2007

Abstract

A model of microstructurally short cracks that accounts for random grain geometry and crystallographic orientations is coupled with crystal plasticity constitutive model. A short crack is then inserted in the slip plane in one of the grains at the model top boundary and extended into one of the available slip planes of the neighboring grain at monotonic remote load of $0.96R_{p0.2}$. Crack tip opening (CTOD) and sliding (CTSD) displacements are then calculated for several different crystallographic orientations and crack lengths. As the crack is contained in a single grain the crystallographic orientation of the neighboring grain can change the crack tip displacements by up to 26%, however, the displacements change by up to a factor of 10, once the crack is extended beyond the grain boundary into the next grain. Significant CTSD values were observed in all the analyzed cases pointing to mixed mode loading. Another important observation is that the random crystallographic orientations of grains beyond the first two crack-containing grains affect the CTOD by a factor of up to 4.4. This effect decreases slightly with increased crack length.

Keywords: Short cracks; Crystallographic orientations; Crack tip displacements; Polycrystalline material; Crystal plasticity

1. Introduction

Microstructurally short cracks behave differently from the long ones. Their propagation rate and path is strongly influenced by local microstructural features such as grain boundaries, crystallographic orientations, inclusions, voids and material phases, etc. [1,2]. Often initiated from persistent slip bands these cracks propagate on the slip planes, creating zigzag patterns [3–5] when changing the slip plane. The crack tip loading is therefore generally mixed mode with strong shear component. All these influence result in a variable crack propagation rates. Vašek [6] for example observed that crack propagation rates may vary significantly for nominally identical cracks.

When creating models of such short cracks care should be taken to incorporate mentioned microstructural features. In recent years several authors applied crystal plasticity material models [7–9] but without the explicit grain shape modeling. Several works use rectangular grain shapes [10,11]. Random grain geometry and crystal plasticity have been used in [12] where calculated *J*-integral values are compared with the isotropic case while in [13] scatter of the *J*-integral values has been determined. Both works deal with intergranular cracks.

In authors' previous studies a combination of random grain geometry and crystal plasticity was used to study the crack tip slip activity and the influence of formation of shear bands on the crack tip displacements [14]. For a bicrystal configuration the preferential slip plane was determined in [15]. Fixed crack length was used in both works. The present study, however, investigates the influence of crystallographic orientations on the crack tip displacements for an advancing crack, including cases where the crack passes the grain boundary. The relation between the crack length, crack tip displacements and their spread due to the random grain orientations is studied. Specifically, we

* Corresponding author. Tel.: +386 (1) 5885 290; fax: +386 (1) 5885 377.
E-mail address: Igor.Simonovski@ijs.si (I. Simonovski).

0142-1123/$ - see front matter © 2007 Published by Elsevier Ltd.
doi:10.1016/j.ijfatigue.2007.01.030

want to see the way in which random grain orientations change the crack tip displacements with the increased crack length.

2. Model description

2.1. Constitutive model

Monocrystal's elastic behaviour is generally anisotropic and is governed by the generalized Hooke's law, $\sigma^{\mathrm{e}}_{ij} = C_{ijkl}\epsilon^{\mathrm{e}}_{kl}$, where σ^{e}_{ij} represents the second-rank elastic stress tensor, C_{ijkl} the fourth-rank stiffness tensor and $\epsilon^{\mathrm{e}}_{kl}$ the second-rank elastic strain tensor. The number of independent elastic constants for a cubic crystal system is 3.

The material's plastic behaviour at the grain level is modeled with crystal plasticity theory [16,17] with an overview given below. Further details on the kinematics are given in [18]. The basic assumption is that the material flows through the crystal lattice via dislocation motion, while the lattice itself, with material embedded on it, undergoes elastic deformations and rotations. The plastic deformation of a monocrystal is assumed to arise solely from simple shear on a specific set of slip planes, see Fig. 1 with projections given in Fig. 2. Deformation by other mechanisms such as for example diffusion, twinning and grain boundary sliding is currently not taken into the account. The total deformation gradient is

$$F_{ij} = F^{*}_{ik} \cdot F^{\mathrm{p}}_{kj}, \tag{1}$$

where F^{*}_{ik} is the elastic part associated with stretching and rotation of the lattice while F^{p}_{kj} is the part of the total deformation gradient due solely to slip. The velocity gradient in the current state is given by a standard formula

$$L_{ij} = \dot{F}_{ik} \cdot F^{-1}_{kj} = D_{ij} + \Omega_{ij} \tag{2}$$

and can be expressed as a sum of the symmetric rate of stretching D_{ij} and antisymmetric spin tensor Ω_{ij}. D_{ij} and Ω_{ij} can be further decomposed into plastic parts (D^{p}_{ij} and Ω^{p}_{ij}) and lattice or elastic parts (D^{*}_{ij} and Ω^{*}_{ij}), i.e., $D_{ij} = D^{*}_{ij} + D^{\mathrm{p}}_{ij}$

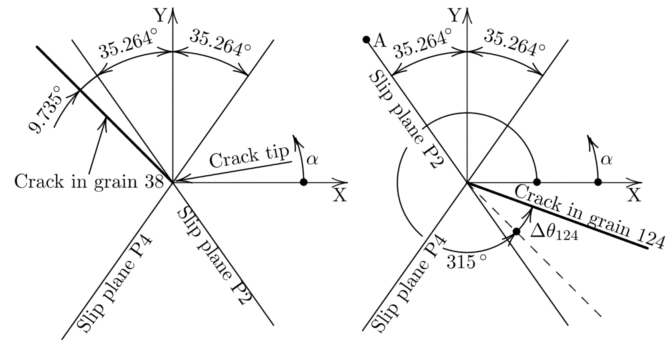

Fig. 2. Relation between the crack plane and slip planes P2 and P4 at crystallographic orientation of $\alpha = 0°$. Left: crack in grain 38. Right: an example of a crack in grain 124.

and $\Omega_{ij} = \Omega^{*}_{ij} + \Omega^{\mathrm{p}}_{ij}$. Now, the plastic part of the velocity gradient in the current state can be expressed as

$$D^{\mathrm{p}}_{ij} + \Omega^{\mathrm{p}}_{ij} = \sum_{\alpha} \dot{\gamma}^{(\alpha)} s^{(\alpha)}_i m^{(\alpha)}_j, \tag{3}$$

where the summation is performed over all active slip systems, (α), defined by their normal $m^{(\alpha)}_i$ and a shearing direction, $s^{(\alpha)}_i$. $\dot{\gamma}^{(\alpha)}$ represents the shear rate. The cumulative slip, γ, is defined as,

$$\gamma = \sum_{\alpha} \int_0^t |\dot{\gamma}^{(\alpha)}| \mathrm{d}t. \tag{4}$$

Plastic strain rate is then obtained from the symmetric part of Eq. (3)

$$\dot{\epsilon}^{\mathrm{p}}_{ij} = \sum_{\alpha} \frac{1}{2} \dot{\gamma}^{(\alpha)} (s^{(\alpha)}_i m^{(\alpha)}_j + s^{(\alpha)}_j m^{(\alpha)}_i). \tag{5}$$

The constitutive relation of the elastic–plastic monocrystal is now given in terms of stress and strain rates as, $\dot{\sigma}_{ij} = C_{ijkl}(\dot{\epsilon}_{kl} - \dot{\epsilon}^{\mathrm{p}}_{kl})$ [19]. It is assumed that the shear rate $\dot{\gamma}^{(\alpha)}$ depends on the stress only via the Schmid resolved shear stress, Eq. (6). This is a reasonable approximation at room temperature and for ordinary strain rates and pressures [19]. Yielding is then assumed to take place when

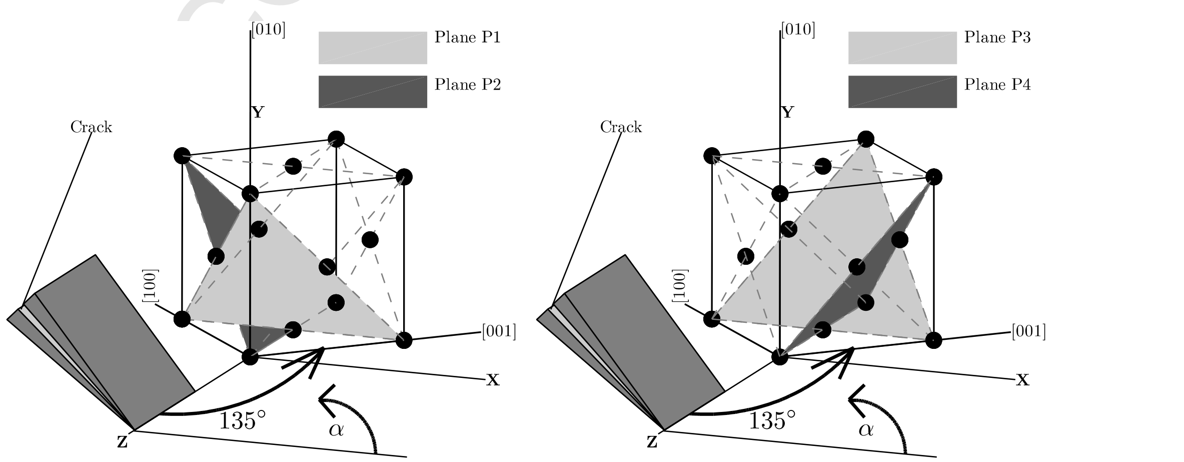

Fig. 1. Relation between the slip planes of a face centered cubic material and the crack for $\alpha = 0°$. The crack plane is aligned with slip plane P2.

Please cite this article in press as: Simonovski I, Cizelj L, The influence of grains' crystallographic orientations on advancing ..., Int J Fatigue (2007), doi:10.1016/j.ijfatigue.2007.01.030

the Schmid resolved shear stress exceeds the critical shear stress τ_0.

$$\dot{\gamma}^{(\alpha)} = \dot{a}^{(\alpha)} \left(\frac{\tau^{(\alpha)}}{g^{(\alpha)}}\right) \left|\frac{\tau^{(\alpha)}}{g^{(\alpha)}}\right|^{n-1}, \quad \tau^{(\alpha)} = s_i^{(\alpha)} \sigma_{ij} m_j^{(\alpha)}, \tag{6}$$

$\dot{a}^{(\alpha)}$ represents the reference strain rate, n is the strain rate-sensitivity parameter and $g^{(\alpha)}$ is the current strain-hardened state of the crystal. In the limit, as n approaches infinity, this power law approaches that of a rate-independent material. The current strain-hardened state $g^{(\alpha)}$ can be derived from,

$$\dot{g}^{(\alpha)} = \sum_{\beta} h_{\alpha\beta}, \quad \dot{\gamma}^{(\beta)}, \tag{7}$$

where $h_{\alpha\beta}$ are the slip-hardening moduli defined by the adopted hardening law. In this work Peirce et al. hardening law is used [20], where self-hardening moduli $h_{\alpha\alpha}$ are defined by:

$$h_{\alpha\alpha} = h(\gamma) = h_0 \text{sech}^2 \left|\frac{h_0 \gamma}{\tau_s - \tau_0}\right|, \quad \text{sech} = 1/\cosh\,. \tag{8}$$

Here h_0 stands for the initial hardening modulus, τ_0 is the yield stress (equal to the initial value of the current strength $g^{(\alpha)}(0)$) and τ_s a reference stress where large plastic flow initiates. The latent-hardening moduli $h_{\alpha\beta}$ are determined as

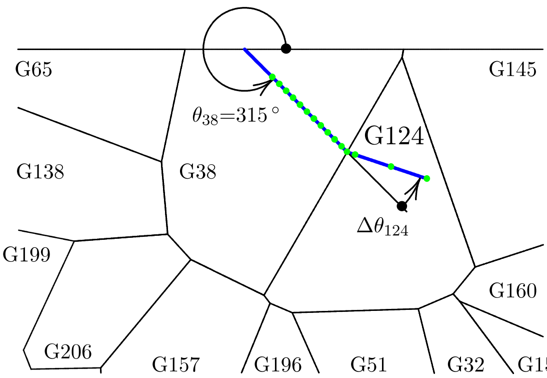

Fig. 4. Definitions of grain numbers, crack direction and deflection angles, θ_{38} and $\Delta\theta_{124}$. Dots indicate most of the used crack lengths.

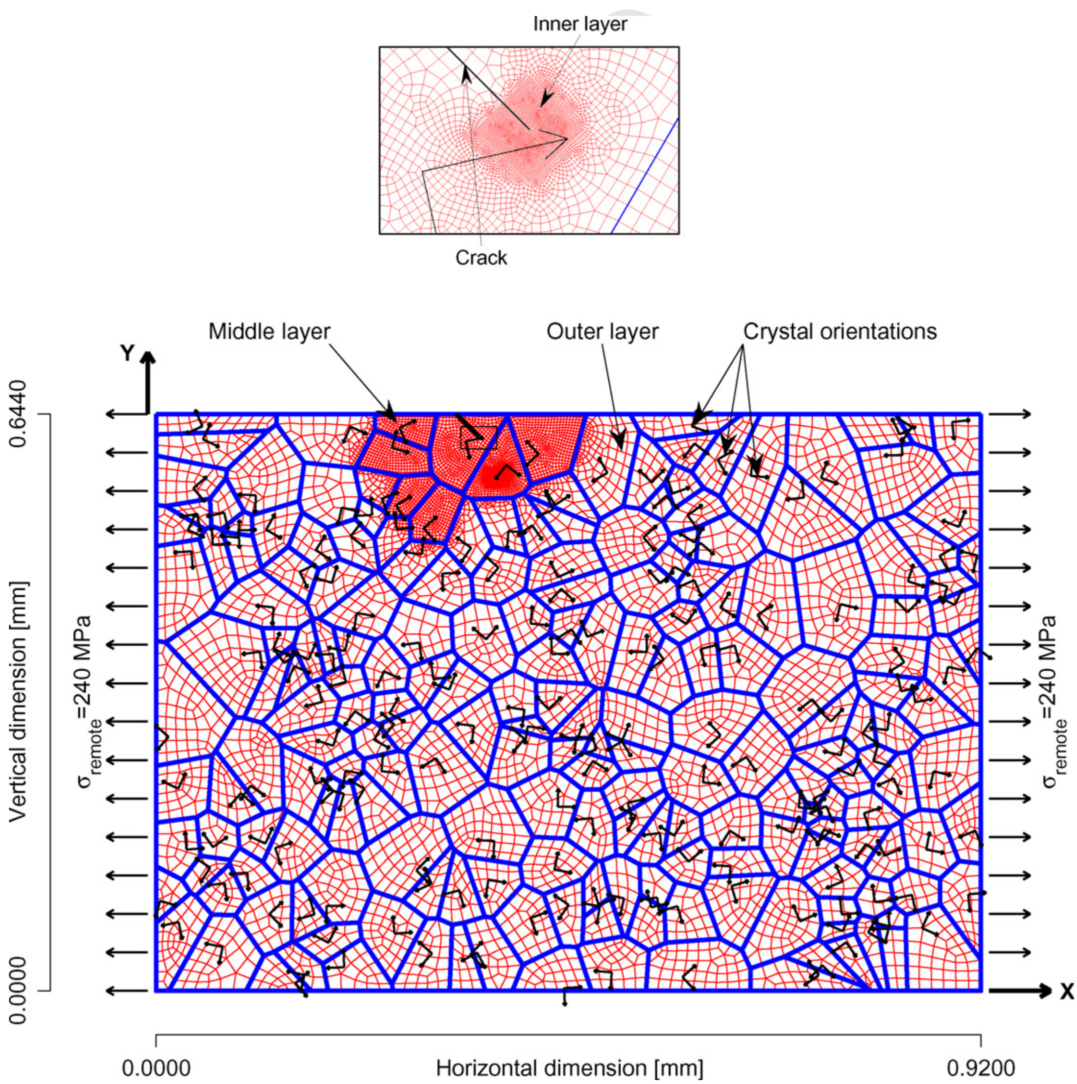

Fig. 3. The finite element model. Details of the crack tip mesh are shown in the insert.

Please cite this article in press as: Simonovski I, Cizelj L, The influence of grains' crystallographic orientations on advancing ..., Int J Fatigue (2007), doi:10.1016/j.ijfatigue.2007.01.030

$h_{\alpha\beta} = qh(\gamma)$, $(\alpha \neq \beta)$, where q is a hardening factor. This model was implemented as a user-subroutine into the finite element code ABAQUS [21] and includes versions for small deformation theory and rigorous theory of finite-strain and finite-rotation. The latter was used in this work.

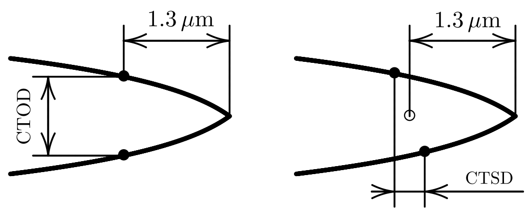

Fig. 5. Definition of the CTOD and CTSD.

Table 1
Crystallographic orientations for grain 124 and corresponding crack deflection angles

Crystallographic orientation		Crack deflection angle $\Delta\theta_{124}$	
α_{38}	α_{124}	Crack in SP2	Crack in SP4
9.735°	36.264°	26.528°	−44°
9.735°	56.264°	46.528°	−24°
9.735°	64.264°	54.528°	−16°
9.735°	70.264°	60.528°	−10°
9.735°	80°	70.264°	−0.264°

2.2. Layout of structural model

The structural model is a planar rectangular aggregate consisting of 212 randomly sized and shaped grains. The aggregate is a planar Voronoi tessellation generated using code VorTESS [22]. The model results in an average grain size of about 53 μm which is in agreement with published values for 316L steel, reported to be between 50 and 80 μm. Standard deviation of grain sizes divided by average grain size is reported to be 0.32 μm/μm [23]. 316L has relatively weak morphological texture, with elongation of grains in the rolling direction of about 20% [24]. This effect was, however, not accounted for in our model. 316L is an austenitic steel with a face centered body structure and is used in certain nuclear power plant piping systems.

The finite element model of the grain structure with a crack is presented in Fig. 3. Each grain is subdivided into 8-noded, reduced-integration, plane strain finite elements. The mesh is composed out of inner, middle and outer layer. The inner layer is defined by a rectangle of size 10 × 10 μm, with crack tip at its center. Average element size in the inner layer of 0.125 μm is achieved by assigning 80 elements along each of the rectangle's sides and 40 elements along the part of the crack pertaining to the inner layer. Crack-containing grain (except the area of the inner layer) and all the grains that have a common border with the crack-containing grains compose the middle layer. Average element size in this layer is 2.5 μm. Grains beyond the

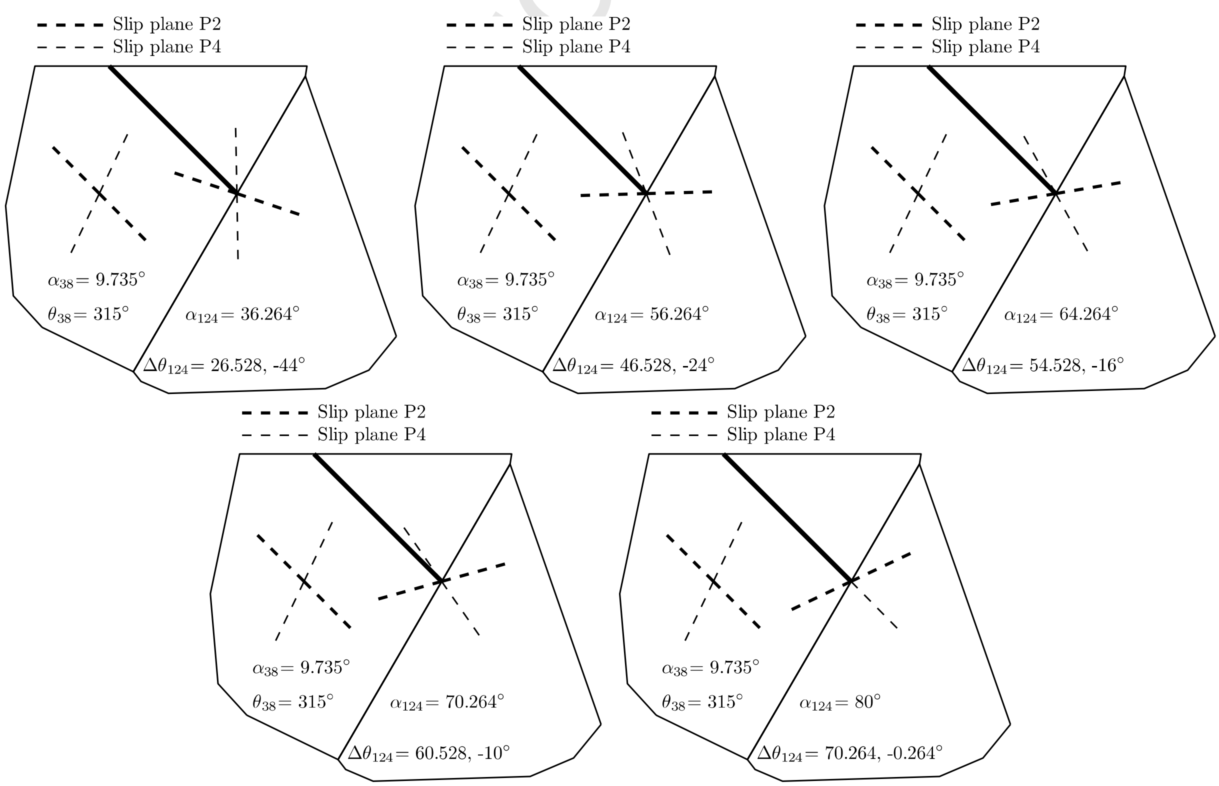

Fig. 6. Applied crystallographic orientations of grains 38 (9.735°) and 124 (36.264°, 56.264°, 64.264°, 70.264° and 80°). Two possible crack extension deflections are indicated with two values of $\Delta\theta_{124}$.

Please cite this article in press as: Simonovski I, Cizelj L, The influence of grains' crystallographic orientations on advancing ..., Int J Fatigue (2007), doi:10.1016/j.ijfatigue.2007.01.030

middle layer compose the outer layer. Average element size in this layer is 13 μm. The finite element meshing of the grains in this layer is automatic and follows procedures outlined in [25].

To avoid violations of finite element shape constraints, only a subset of “meshable” Voronoi tessellations has been considered in the analysis. The “meshable” tessellations basically assume reasonably small aspect ratios of cord lengths. Further details are available in [25]. Such approach essentially prevents use of tessellations with very small grains.

Each grain is assumed to behave as a monocrystal governed by the anisotropic elasticity and crystal plasticity models as described in the previous section. The number of grains included in the model is not sufficient to result in a size-independent macroscopic response of the aggregate (representative volume element). The overall global response of the aggregate will therefore still slightly depend on the applied set of crystallographic orientations and grain sizes and shapes. Should the aggregate be larger than the representative volume element, its overall response would not depend on the applied set of crystallographic orientations or grain sizes and shapes. However, the experience with similar simulations shows that the error caused by this omission is limited to about 5% [26].

2.2.1. The crack and crystallographic orientations

A short inclined surface crack is introduced in the model. Crack is placed in a slip plane to mimic Stage I fatigue crack. This is achieved by first setting the angle between the crystallographic [1 0 0] direction and the macroscopic X-axis of all crystals in the model to 135° as shown in Fig. 1. The projections of slip planes are given in Fig. 2. This results in a planar slip system model compatible with the planar macroscopic model. Next, each crystal is rotated around the global Z-axis by an angle α, obtained by a random generator with uniform distribution. We will refer to this angle as crystallographic orientation. As reported in [24] 316L steel has a fairly strong crystallographic texture with a great number of grains having normal direction close to $\langle 1\,1\,1\rangle$ and $\langle 1\,0\,0\rangle$ direction. $\langle 1\,0\,0\rangle$ direction is less pronounced while only a few grains exhibit a normal close to the $\langle 1\,1\,0\rangle$ direction. This texture was not taken into account because: (a) our intention is to maximize the scatter of the results due to crystallographic orientations, including the texture would decrease the scatter and (b) the effect of the texture is considered small compared to the 2D approximation of the aggregate used in this paper.

Crystallographic orientation of the grain 38 (the first crack-containing grain, see Fig. 4 for grain numbers) is set to 9.375° so that the crack falls into the slip plane P2, left-hand side of Fig. 2. For the face centered cubic material the angle between the slip planes P2 and P4 is $2 \times 35.264°$. Crystallographic orientation of the grain 124 (second crack-containing grain) has to be such that the crack is either in slip plane P2 or P4. Crack direction in grain 124 is $315° + \Delta\theta_{124}$, where $\Delta\theta_{124}$ is crack deflection angle. Positive direction of $\Delta\theta_{124}$ is in counter clockwise direction. For the crack to fall into the slip plane P2, we select to rotate the crystal in the counter clockwise direction until the point A on the slip plane P2 falls onto the crack, see right-hand side of Fig. 2. This condition is satisfied when $315° + \Delta\theta_{124} = \alpha_{124_{P2}} + 90° + 35.264° + 180°$. Required crystallographic orientation of grain 124, for the crack to fall into the slip plane P2, is then given by Eq. (9). Similar arguments can be applied to obtain the crystallographic orientation of grain 124 for the crack to fall into the slip plane P4, Eq. (10).

$$\alpha_{124_{P2}} = (315° + \Delta\theta_{124}) - 180° - 90° - 35.264°, \quad (9)$$

$$\alpha_{124_{P4}} = (315° + \Delta\theta_{124}) - 180° - 90° + 35.264°. \quad (10)$$

The crack tip opening (CTOD) and sliding (CTSD) displacements are calculated at a distance of 2.5% of the average grain size behind the crack tip (i.e. $0.025 \times 52.9 = 1.3$ μm), see Fig. 5. This is consistent with examples found in the literature [11,27].

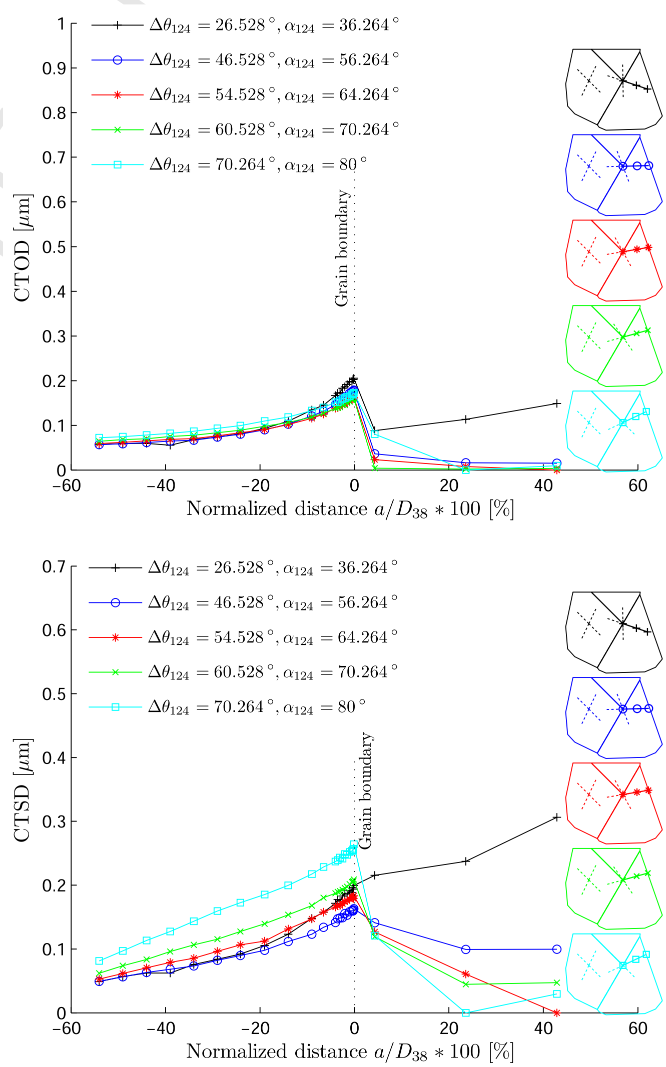

Fig. 7. The influence of different crystallographic orientations of grain 124 on the crack tip displacements. Crack in grain 124 is placed in slip plane P2.

Please cite this article in press as: Simonovski I, Cizelj L, The influence of grains' crystallographic orientations on advancing ..., Int J Fatigue (2007), doi:10.1016/j.ijfatigue.2007.01.030

Extensive mesh sensitivity study was performed in [28] resulting in the optimal mesh shown in Fig. 3. The applied mesh is expected to underestimate CTOD and CTSD by about 4.6% and 8.4% [28], respectively, which is deemed sufficient for the presented analysis.

2.2.2. Loading and boundary conditions

The applied macroscopic loading and boundary conditions are illustrated in Fig. 3. The left and right edges are loaded in macroscopic monotonic uniaxial tension up to a maximum load of $0.96R_{p0.2}$ (240 MPa) with zero shear traction. This load is sufficient to trigger slip systems activity in all cases analyzed. The upper and lower edges are traction free. Prevention of rigid body movement is also imposed.

2.2.3. Material parameters

Elastic constants for AISI 316L single crystal were taken from literature [29]: $C_{iiii} = 163{,}680$ MPa, $C_{iijj} = 110{,}160$ MPa, $C_{ijij} = 100{,}960$ MPa. Crystal plasticity parameters are also taken from [29] and are as follows: $h_0 = 330$ MPa, $\tau_s = 270$ MPa, $\tau_0 = 90$ MPa, $n = 55$, $q = 1.0$ and $\dot{a}^{(\alpha)} = 0.001$. The material parameters in [29] were obtained by fitting the macroscopic response of a polycrystalline model (macroscopic equivalent stress $\langle\sigma_{ij}\rangle$ and strain $\langle\epsilon_{ij}\rangle$, estimated using volume averaging) to the measured true stress–strain curve of a polycrystalline specimen. Mean values correspond quite well with the experimental data. The two times standard deviation of the stress values at specific strains is on average 21 and 16.2 MPa for different grain geometries and crystallographic orientations, respectively.

3. Results

3.1. Variable crack lengths

In this section we examine crack tip displacements and accumulated slip around the crack tip as the crack is extended from the first into the second grain. The sizes of

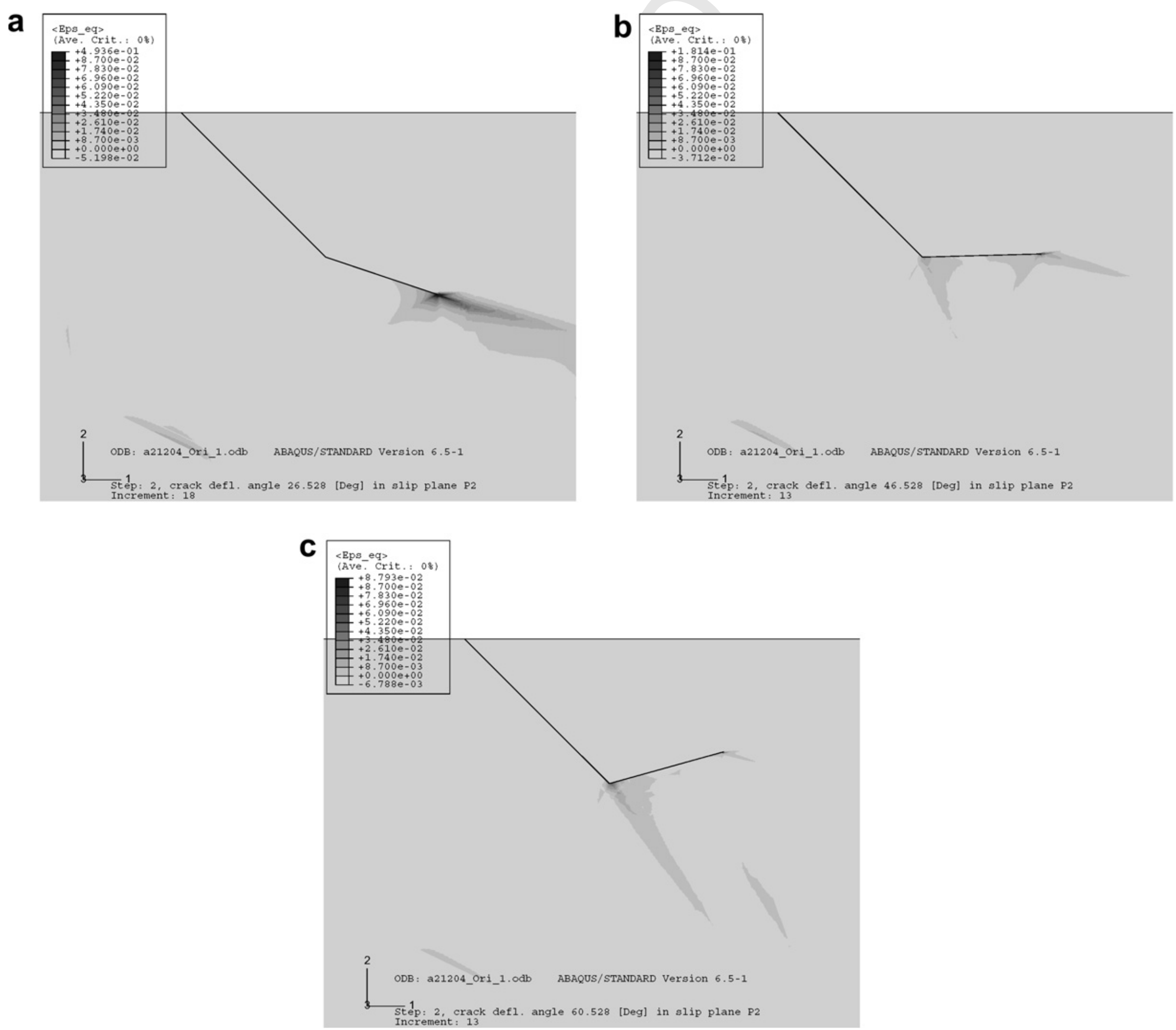

Fig. 8. Increasing the crack deflection angle results in a shift of position of maximal equivalent strain $<\epsilon_{eq}>$ from the crack tip point to the crack kink point. Crack in grain 124 is placed in slip plane P2.

these two grains can influence the crack tip displacements. A larger grain with a favourable orientation will tend to increase the crack tip displacements compared to a smaller grain with the same orientation [14]. In all cases we assume a Stage I crack, which propagates only through slip planes. The crystallographic orientation of the grain 38 is rotated in anti-clockwise direction by an angle $\alpha = 9.735°$ so that the crack at an angle of $\theta_{38} = 135°$ falls onto the slip plane P2. Let $D_{38} = 70.87$ μm stand for the size of the grain 38, estimated as a square root of its area. We created a series of models with embedded stationary cracks of different lengths. Crack length in the grain 38 varies from $0.25D_{38}$ up to $0.739D_{38}$ which is almost on the grain boundary. Once the crack extends across the grain boundary (into the grain 124) its length is up to $0.5D_{124}$. $D_{124} = 60.78$ μm is the size of the grain 124, estimated as a square root of its area. Several crystallographic orientations of the grain 124 are used while placing the crack in either slip plane P2 or P4, see Table 1. Fig. 6 shows the corresponding crystallographic orientations. The orientations of all other grains are random.

Fig. 7 shows the CTOD and CTSD displacements for crack in grain 124 placed in the slip plane P2. Abscissa's value of 0 indicates the grain boundary. One can see that different crystallographic orientations of grain 124 change CTOD values by 26% for the case with the shortest crack. As the crack is extended into the grain 124 this effect becomes much more pronounced. This is to be expected since the crack has to change its direction at the grain boundary. It was observed that when the crack direction turns upward to follow the slip plane P2, the maximal equivalent strain (Mises equivalent strain), $\langle \epsilon_{eq} \rangle$, gradually shifts from the crack tip to the crack kink point, see Fig. 8. This results in up to 10 times smaller crack tip displacements as the crack crosses the grain boundary. Another important observation is that in all analyzed cases significant CTSD values were observed. Cracks are therefore of mixed mode loading.

Fig. 9 shows crack tip displacements when the crack in grain 124 is placed in the slip plane P4. In these cases the crack in grain 124 can be almost perpendicular to the external load. In fact, we see that the closer the crack extension (in the grain 124) is to being perpendicular to the external load, larger the CTODs and lower the CTSDs are. This would suggest that among all the available slip planes the crack would probably propagate through the slip plane that is more perpendicular to the external load. This is also in line with well known observation where small crack gradually transitions form Stage I to Stage II where its direction is perpendicular to the external load.

Some models of microstructurally short cracks assume that the crack propagation rate is associated with the amount of accumulated plastic displacement along the slip system in front of the crack tip [30]. We therefore calculated the cumulative slip, γ, for elements within the inner

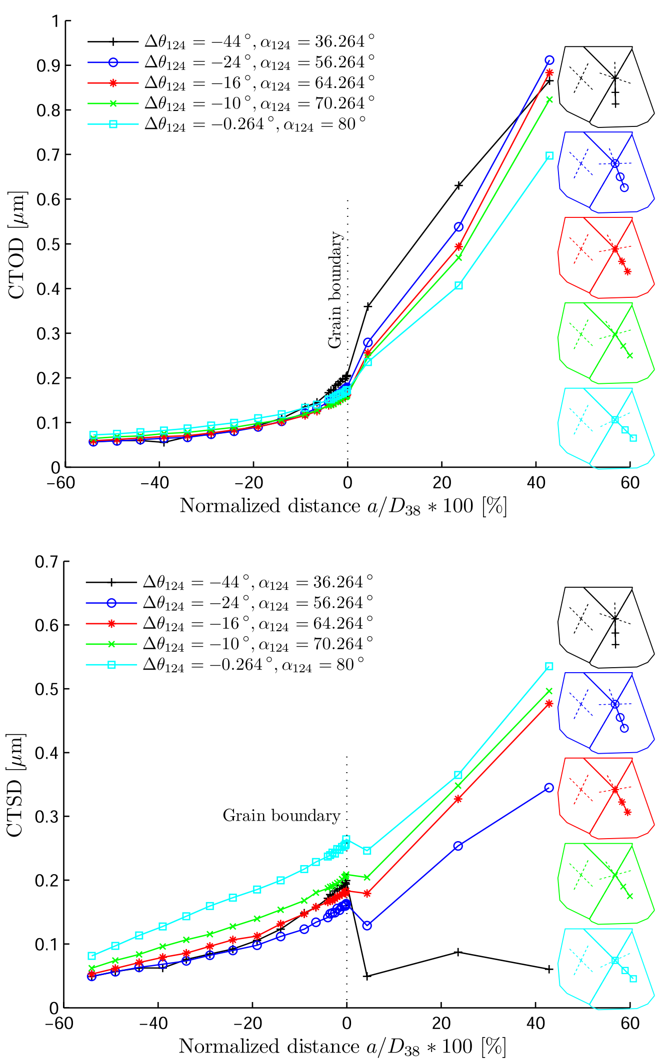

Fig. 9. The influence of different crystallographic orientations of grain 124 on the crack tip displacements. Crack in grain 124 is placed in slip plane P4.

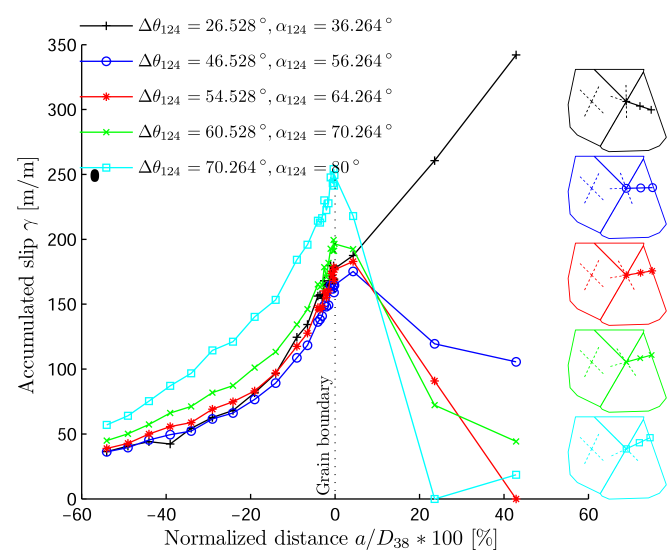

Fig. 10. Cumulative slip around the crack tip. Crack in grain 124 is paced in slip plane P2.

Please cite this article in press as: Simonovski I, Cizelj L, The influence of grains' crystallographic orientations on advancing ..., Int J Fatigue (2007), doi:10.1016/j.ijfatigue.2007.01.030

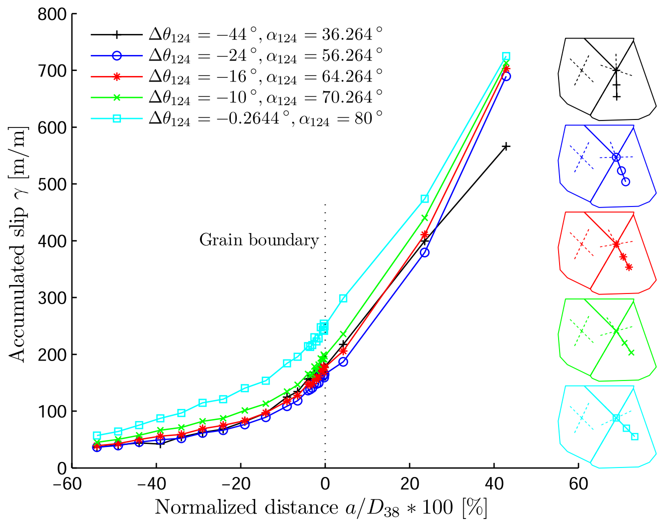

Fig. 11. Cumulative slip around the crack tip. Crack in grain 124 is placed in slip plane P4.

layer of elements around the crack tip, see the insert of Fig. 3. Figs. 10 and 11 show the accumulated slip when placing the crack in the grain 124 in either slip plane P2 or P4. The accumulated slip steadily increases until the crack comes into the vicinity of grain boundary. Beyond the grain boundary the orientation of the crack (defined by the crystallographic orientation) is very important for the accumulated slip. For a crack in slip plane P2, the accumulated slip decreases since the crack turns upwards, away from being perpendicular to the external load. Opposite is true for a crack in slip plane P4. One can see fairly good correlation of the accumulated slip with the crack tip displacements, suggesting that we could formulate a crack propagation criterion based on CTOD as well.

3.2. The influence of random crystallographic orientations

To evaluate the influence of random crystallographic orientations on the CTOD we generated 100 cases where for each fixed orientation of grains 38 (9.735°) and 124 (36.264°, 56.264°, 64.264°, 70.264° and 80°) all other grains were randomly oriented. This was done for two different crack lengths: (a) crack located entirely in the grain 38 with crack length $0.5D_{38}$ and (b) crack extended up to half grain 124 size ($0.5D_{124}$). Crack in grain 124 was placed in slip plane P4. For each case a cumulative probability (distribution) function was calculated. Cumulative probability function, e.g. $F(x)$, is defined as a probability that an observed value (in our case calculated CTOD value) is less than or equal to x. The corresponding results are presented in Figs. 12 and 13. For a crack located entirely in grain 38 we see that different lines are very close to each other. This suggests that the orientation of the grain 124 has a relative small effect on CTOD values when the crack is contained in the first cracked grain (38). However, the scatter of the results along the abscissa shows that the orientations of grains beyond grains 38 and 124 have a significant impact. Changing the orientations of these grains resulted in a scatter of CTOD values by a factor of 4.4.

The impact of the grain's 124 orientation, however, increases once the crack is extended into the grain 124. This can be deduced from a larger distance between different lines in Fig. 13. On the other hand, the impact of (orientations of) grains beyond grains 38 and 124 on CTOD values decreases, manifesting itself in decreased scatter of values along abscissa-3.3 compared to 4.4 for a previous case. Two interlinked factors should also be mentioned once the crack is extended into the grain 124. The first is crack deflection. Larger CTODs are obtained when the crack extension in grain 124 is more perpendicular to the external

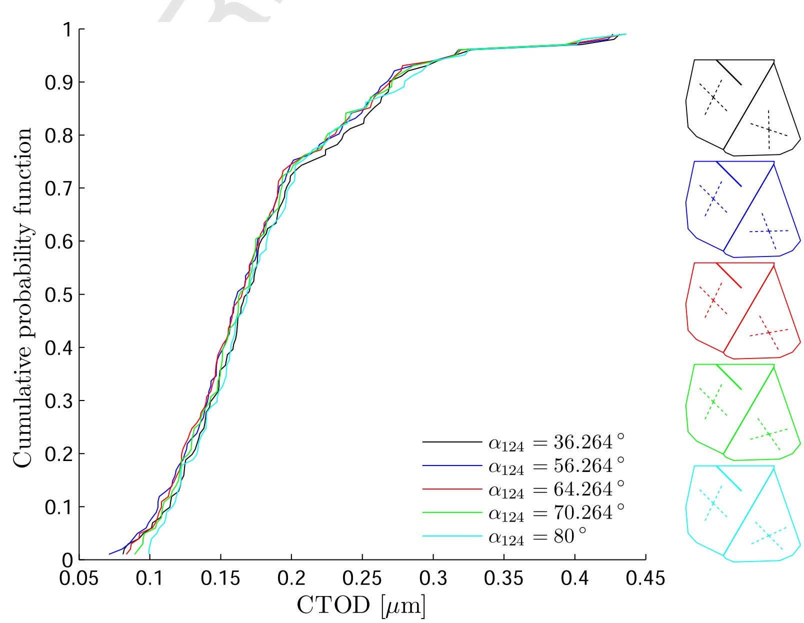

Fig. 12. CTOD histograms for a crack contained in grain 38. Crack length is $0.5D_{38}$.

Please cite this article in press as: Simonovski I, Cizelj L, The influence of grains' crystallographic orientations on advancing ..., Int J Fatigue (2007), doi:10.1016/j.ijfatigue.2007.01.030

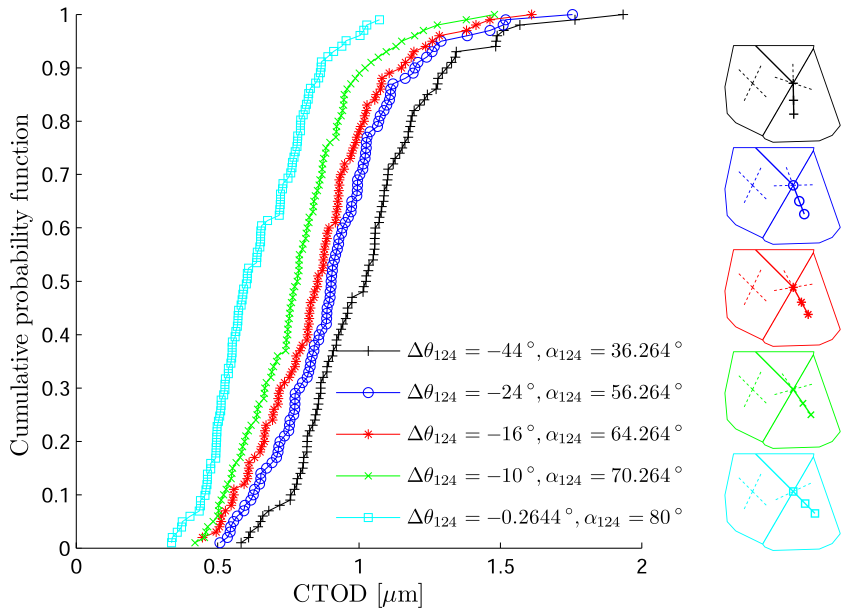

Fig. 13. CTOD histograms for crack in grain 124 and placed in slip plane P4. Crack length in grain 124 is $0.5D_{124}$.

load. Additionally, the crystallographic orientation also affects the stiffness of grain 124. At $\alpha_{124} = 36.264°$ grain 124 has the lowest Schmid factors among the analyzed configurations. However, since the crack in this case is more perpendicular to the external load, the CTODs are the highest. As we increase the α_{124}, Schmid values increase, but the CTODs decrease since the crack extension moves away from being perpendicular to the external load. The crack extension direction in this case seems to be the main factor influencing the CTOD.

4. Conclusions

A model of microstructurally short cracks that accounts for random grain geometry and crystallographic orientations has been coupled with crystal plasticity constitutive model. This models is used to study the influence of variable crack length on crack tip displacements for different grain orientations. In all the analyzed cases the crack tip displacement increased with larger crack, if the crack is contained within the first crack-containing grain.

Second crack-containing grain changes the CTOD by values by 26% for the case with the shortest crack. As the crack is extended into the second crack-containing grain it has to change its direction to follow the available slip plane. The closer the slip plane is to being perpendicular to the external load the larger the CTODs are. Further away the slip plane is from this position, lower the CTODs are. In one of these cases this resulted in a CTOD decrease of a factor 10.

In all analyzed cases significant CTSD values were observed. Cracks are therefore of mixed mode loading.

The spread of the CTODs due to the random crystallographic orientations of grains decreases with increased crack length. The ratio between maximal and minimal CTOD is 4.4 if the crack is contained in the first grain. When the crack is extended into the second grain this ratio is reduced to still significant 3.3. With further increase of the crack length the crack would become less and less depended upon the local microstructural features so the ratio would continue to decrease.

Finally, the model itself needs additional development. Primarily, the crystal plasticity material model needs to be developed further to account for certain aspects of material cyclic behaviour. At a first stage elastic unloading should be implemented whereas in later stages also more complex effects such as Bauschinger effect, cyclic hardening and softening should be considered.

References

[1] Miller KJ. The behaviour of short fatigue cracks and their initiation. Part II-A general summary. Fatigue Fract Eng Mater Struct 1987;10(2):93–113.
[2] Hussain K. Short fatigue crack behaviour and analytical models: a review. Eng Fract Mech 1997;58(4):327–54.
[3] Suresh S. Fatigue of materials. Cambridge University Press; 1991.
[4] Andersson H, Persson C. In situ SEM study of fatigue crack growth behaviour in IN718. Int J Fatigue 2004;26(3):211–9.
[5] Hansson P, Melin S. Dislocation-based modelling of the growth of a microstructurally short crack by single shear due to fatigue loading. Int J Fatigue 2005;27(4):347–56.
[6] Vašek A, Polák J, Obrtlík L. Fatigue damage in two-step loading of 316L steel. II. Short crack growth. Fatigue Fract Eng Mater Struct 1996;19(2–3):157–63.
[7] Gall K, Sehitoglu H, Kadioglu Y. FEM study of fatigue crack closure under double slip. Acta Mater 1996;44(10):3955–65.
[8] Gall K, Sehitoglu H, Kadioglu Y. Plastic zones and fatigue-crack closure under plane-strain double slip. Metall Mater Trans A 1996;27A:3491–501.
[9] Potirniche GP, Daniewicz SR, Newman Jr JC. Simulating small crack growth behaviour using crystal plasticity theory and finite element analysis. Fatigue Fract Eng Mater Struct 2004;27(1):59–71.

Please cite this article in press as: Simonovski I, Cizelj L, The influence of grains' crystallographic orientations on advancing ..., Int J Fatigue (2007), doi:10.1016/j.ijfatigue.2007.01.030

[10] Tvergaard V, Wei Y, Hutchinson JW. Edge cracks in plastically deforming surface grains. Eur J Mech A–Solid 2001;20(5):731–8.
[11] Potirniche GP, Daniewicz SR. Analysis of crack tip plasticity for microstructurally small cracks using crystal plasticity theory. Eng Fract Mech 2003;70(13):1623–43.
[12] Cizelj L, Kovše I. Short intergranular cracks in the piecewise anisotropic continuum model of the microstructure. In: International conference nuclear energy in central Europe 2001. Ljubljana: Nuclear Society of Slovenia; 2001.
[13] Cizelj L, Riesch-Oppermann H. Towards growth model for short intergranular cracks in elastoplastic polycrystalline aggregate. In: Fontevraud 5: proceedings of the international symposium contribution of materials investigation to the resolution of problems encountered in pressurized water reactors, vol. 1; 2002, p. 196–203.
[14] Simonovski I, Nilsson K-F, Cizelj L. Crack tip displacements of microstructurally small cracks in 316L steel and their dependance on crystallographic orientations of grains. Fatigue Fract Eng Mater Struct, [in press].
[15] Simonovski I, Nilsson K-F, Cizelj L. The influence of crystallographic orientation on crack tip displacements of microstructurally small, kinked crack crossing the grain boundary. Comput Mater Sci, [in press].
[16] Hill R, Rice JR. Constitutive analysis of elastic–plastic crystals at arbitrary strain. J Mech Phys Solids 1972;20(6):401–13.
[17] Rice JR. On the structure of stress–strain relations of time-dependent plastic deformation in metals. J App Mech 1970;37:728–37.
[18] Asaro RJ. Crystal plasticity. J App Mech 1983;50:921–34.
[19] Needleman A. Computational mechanics at the mesoscale. Acta Mater 2000;48(1):105–24.
[20] Peirce D, Asaro RJ, Needleman A. Material rate dependence and localized deformation in crystalline solids. Acta Metall 1983;31(12):1951–76.
[21] Huang Y. A user-material subroutine incorporating single crystal plasticity in the ABAQUS finite element program. Technical Report, Harvard University; 1991 (accessible through http://www.columbia.edu/~jk2079/fem/umat_documentation.pdf).
[22] Riesch-Oppermann H. Generation of 2D random Poisson–Voronoi mosaics as framework for micromechanical modeling of polycrystalline materials-algorithm and subroutines description. Technical Report, FZKA 6325, Forschungszentrum Karlsruhe; 1999.
[23] Singh KK, Sangal S, Murty GS. Hall-Petch behaviour of 316L austenitic stainless steel at room temperature. Mater Sci Technol 2002;18(165):165–72.
[24] Mineur M, Villechaise P, Mendez J. Influence of the crystalline texture on the fatigue behavior of a 316L austenitic stainless steel. Mater Sci Eng A 2000;286(2):257–68.
[25] Weyer S, Frohlich A, Riesch-Oppermann H, Cizelj L, Kovač M. Automatic finite element meshing of planar Voronoi tessellations. Eng Fract Mech 2002;69(8):945–58.
[26] Kovač M. Influence of microstructure on development of large deformations in reactor pressure vessel steel. Ph.D. thesis. University Of Ljubljana, Faculty 0f Mathematics And Physics; 2004 (accessible through http://www2.ijs.si/~podiprt/PhD/KovacPhD2004.pdf).
[27] Bennett VP, McDowell DL. Crack tip displacements of microstructurally small surface cracks in single phase ductile polycrystals. Eng Fract Mech 2003;70(2):185–207.
[28] Simonovski I. Mechanisms for thermal fatigue initiation and crack propagation in NPP components. 2nd Mid-term report, Technical Report, Jožef Stefan Institute, DG-JRC, Institute for Energy; 2005 (accessible through http://www.rcp.ijs.si/isimonovski/Papers/Simonovski_2005_2.pdf).
[29] Simonovski I, Nilsson K-F, Cizelj L. Material properties calibration for 316L steel using polycrystalline model. In: ICONE 13: proceedings of the 13th international conference on nuclear engineering. Beijing; 2005.
[30] Lillbacka R, Johnson E, Ekh M. A model for short crack propagation in polycrystalline materials. Eng Fract Mech 2006;73(2):223–32.

Please cite this article in press as: Simonovski I, Cizelj L, The influence of grains' crystallographic orientations on advancing ..., Int J Fatigue (2007), doi:10.1016/j.ijfatigue.2007.01.030